

Pairing transitions in a binary Bose gas

Zesheng Shen(沈泽盛) and Lan Yin(尹澜)

Citation: Chin. Phys. B, 2025, 34 (**10**): 106702. DOI: 10.1088/1674-1056/ade075
http://cpb.iphy.ac.cn; http://iopscience.iop.org/cpb

What follows is a list of articles you may be interested in

Three-dimensional ResNet for efficient prediction of ground state phases in multicomponent dipolar spinor BECs

Chengji Liao(廖承继), Tiantian Li(李甜甜), Xiao-Dong Bai(柏小东), and Yunbo Zhang(张云波)
Chin. Phys. B, 2025, 34 (**7**): 076701. DOI: 10.1088/1674-1056/adc7f9

Spinor *F*=1 Bose-Einstein condensates loaded in two types of radially-periodic potentials with spin-orbit coupling

Ji-Guo Wang(王继国), Yue-Qing Li(李月晴), Han-Zhao Tang(唐翰昭), and Ya-Fei Song(宋亚飞)
Chin. Phys. B, 2021, 30 (**10**): 106701. DOI: 10.1088/1674-1056/ac1411

Bose-Einstein condensates under a non-Hermitian spin-orbit coupling

Hao-Wei Li(李浩伟) and Jia-Zheng Sun(孙佳政)
Chin. Phys. B, 2021, 30 (**6**): 066702. DOI: 10.1088/1674-1056/abd7e4

Propagation of dark soliton interacting with domain wall in two immiscible Bose-Einstein condensates

Lang Zheng(郑浪), Yi-Cai Zhang(张义财), Chao-Fei Liu(刘超飞)
Chin. Phys. B, 2019, 28 (**11**): 116701. DOI: 10.1088/1674-1056/ab457e

Vortices in dipolar Bose-Einstein condensates in synthetic magnetic field

Qiang Zhao(赵强) and Qiang Gu(顾强)
Chin. Phys. B, 2016, 25 (**1**): 016702. DOI: 10.1088/1674-1056/25/1/016702

Pairing transitions in a binary Bose gas

Zesheng Shen(沈泽盛) and Lan Yin(尹澜)[†]

School of Physics, Peking University, Beijing 100871, *China*

(Received 26 May 2025; revised manuscript received 3 June 2025; accepted manuscript online 4 June 2025)

The stable Bardeen–Schrieffer–Cooper (BCS) pairing state of a bosonic system has long been sought theoretically and experimentally. Here we propose that a stable BCS state of bosons can be realized in a binary Bose gas with s-wave intra-species repulsion and an inter-species attraction in the mean-field-stable region. We find that above the Bose–Einstein condensation (BEC) transition temperature, there is a phase transition from the normal state to a BCS state driven by inter-species pairing. When the temperature decreases, another phase transition from the BCS state to a mixed state featuring both atomic BEC and inter-species pairing occurs. As the temperature is further lowered, the mixed state is eventually taken over by the pure BEC state. We present the phase diagram of this system and discuss its experimental implications.

Keywords: pairing states, Bose–Einstein condensates

PACS: 67.85.–d, 03.75.Hh

DOI: 10.1088/1674-1056/ade075 **CSTR:** 32038.14.CPB.ade075

1. Introduction

The study of superfluidity and superconductivity has been a cornerstone of modern condensed matter physics. After the experimental realization of Bose–Einstein condensation (BEC),[1,2] ultracold atoms have provided a new platform for these studies. By the Feshbach resonance technique, the interactions between atoms can be tuned, and the BEC–BCS (Bardeen–Schrieffer–Cooper) crossover of fermions[3,4] was experimentally achieved.[5–14] Ever since the BCS theory,[15] whether or not bosons can also form a stable pairing state[16] has remained a crucial problem. In a single-component Bose gas, it was found theoretically that the BCS pairing state is mechanically unstable under attractive interactions. In contrast, under repulsive interactions, each atom can pair with another to form a tightly bound molecule, and these molecules can condense stably below a critical temperature.[17–22] Experimentally, the strong three-body loss process near the Feshbach resonance has posed a major challenge for creating a molecular BEC state.[23–26] In 2021, a molecular BEC was first experimentally observed in a two-dimensional Bose gas with g-wave closed-channel molecules.[27]

In recent years, the binary Bose gas has attracted considerable attention due to the successful experimental realization of quantum droplets.[28–30] In such a system, the inter-species attraction exceeds the geometric mean of the intra-species repulsions. Although the overall mean-field energy is attractive, mechanical stability is restored by the Lee–Huang–Yang (LHY) energy arising from Gaussian fluctuations.[31,32] In the Bogoliubov theory of the quantum droplet, the phonon excitation energy becomes imaginary in the long-wavelength limit, implying an instability. It was later found that the phonon energy is stabilized by higher-order quantum fluctuations.[33–36] In an alternative proposal, the ground state of the quantum droplet is predicted to be a pairing state rather than a BEC state.[37,38]

In this work, we theoretically investigate a dilute binary Bose gas with an inter-species attraction and symmetric intra-species repulsions in the mean-field-stable region, where the overall mean-field energy is repulsive and dominates over the LHY correction, in contrast to the quantum-droplet case where the mean-field energy is attractive and of the same order as the LHY correction. We obtain the phase diagram of this system as shown in Figs. 1 and 2. By studying inter-species pairing self-consistently within the mean-field approximation, we find that a stable BCS state exists above the BEC transition temperature, and turns into the normal state when the temperature rises above a threshold. The pairing state is shown to be stable in the Ginzburg–Landau theory. The energy gap in the excitation spectrum of the BCS state closes as the temperature decreases to a critical value, where a phase transition from the BCS state to a mixed state of atomic BEC and inter-species pairs takes place. The BEC–BCS mixed state is eventually taken over by a pure BEC state at a lower critical temperature. Experimental implications are also discussed at the end.

2. BCS pairing state of a binary Bose gas

2.1. General model

We consider a uniform binary Bose gas described by the Hamiltonian $H = H_0 + H_{\rm I}$. The single-particle Hamiltonian is given by

$$H_0 = \sum_{\boldsymbol{k},i} \varepsilon_{\boldsymbol{k}} c^{\dagger}_{i\boldsymbol{k}} c_{i\boldsymbol{k}}, \tag{1}$$

[†]Corresponding author. E-mail: yinlan@pku.edu.cn

© 2025 Chinese Physical Society and IOP Publishing Ltd. All rights, including for text and data mining, AI training, and similar technologies, are reserved.

and the s-wave interaction term is given by

$$H_{\rm I} = \sum_{\boldsymbol{k}_1\boldsymbol{k}_2\boldsymbol{k}_3,i,j} \frac{g_{ij}}{2V} c^\dagger_{i\boldsymbol{k}_1} c^\dagger_{j\boldsymbol{k}_2} c_{j\boldsymbol{k}_3} c_{i\boldsymbol{k}_1+\boldsymbol{k}_2-\boldsymbol{k}_3}, \tag{2}$$

where V is the volume, $\varepsilon_{\boldsymbol{k}}$ is the kinetic energy $\varepsilon_{\boldsymbol{k}} = \hbar^2\boldsymbol{k}^2/(2m)$, $c_{i\boldsymbol{k}}$ denotes the boson annihilation operator for the i-th component ($i = 1,2$), $g_{ij} = g_{ji} = 4\pi\hbar^2 a_{ij}/m$ is the coupling constant between the i-th and j-th components, and a_{ij} denotes the s-wave scattering length. In the following, we focus on the case with inter-species attraction $a_{12} < 0$ and symmetric intra-species repulsions $a_{11} = a_{22} > 0$ in the mean-field-stable region $|a_{12}| < a_{11}$.

2.2. Mean-field approximation

We consider pairing due to the attractive inter-species interaction and define the pairing order parameter as

$$\Delta = \frac{g_{12}}{V}\sum_{\boldsymbol{k}} \langle c_{1\boldsymbol{k}} c_{2-\boldsymbol{k}}\rangle, \tag{3}$$

where the term with $\boldsymbol{k} = 0$ is negligible in the thermodynamic limit in the absence of a BEC and should be treated separately in the presence of BEC. Here we study the pure BCS state and set the pair amplitude $\sum_{\boldsymbol{k}}\langle c_{1\boldsymbol{k}} c_{2-\boldsymbol{k}}\rangle$ positive without loss of generality, so that Δ is negative. Within the mean-field approximation, which includes both pairing and Hartree–Fock energies, the Hamiltonian in the grand-canonical ensemble is given by

$$H_{\rm B} - \mu N = \sum_{\boldsymbol{k}} (c^\dagger_{1\boldsymbol{k}}, c_{2-\boldsymbol{k}}) \begin{pmatrix} \varepsilon_{\boldsymbol{k}} - \mu' & \Delta \\ \Delta & \varepsilon_{\boldsymbol{k}} - \mu' \end{pmatrix} \begin{pmatrix} c_{1\boldsymbol{k}} \\ c^\dagger_{2-\boldsymbol{k}} \end{pmatrix} + E_{\rm B}, \tag{4}$$

where $E_{\rm B} = -\sum_{\boldsymbol{k}}(\varepsilon_{\boldsymbol{k}} - \mu') - \frac{\Delta^2 V}{g_{12}} - (2g_{11} + g_{12})n^2 V$, μ is the chemical potential, $\mu' = \mu - (2g_{11} + g_{12})n$ is the shifted chemical potential excluding the Hartree–Fock energy, and N is the total number operator.

This mean-field Hamiltonian can be diagonalized using a Bogoliubov transformation, with the quasiparticle excitation energy given by

$$E_{\boldsymbol{k}} = \sqrt{(\varepsilon_{\boldsymbol{k}} - \mu')^2 - \Delta^2}, \tag{5}$$

indicating that the minimum excitation energy exhibits a gap given by $E_0 = \sqrt{\mu'^2 - \Delta^2}$. The shifted chemical potential μ' and the pairing order parameter Δ can be self-consistently determined from the following number and gap equations:

$$n = \int \frac{{\rm d}^3\boldsymbol{k}}{2(2\pi)^3}\left(\frac{\varepsilon_{\boldsymbol{k}} - \mu'}{E_{\boldsymbol{k}} \tanh\frac{\beta E_{\boldsymbol{k}}}{2}} - 1\right), \tag{6a}$$

$$-\frac{m}{4\pi\hbar^2 a_{12}} = \int \frac{{\rm d}^3\boldsymbol{k}}{2(2\pi)^3}\left(\frac{1}{E_{\boldsymbol{k}} \tanh\frac{\beta E_{\boldsymbol{k}}}{2}} - \frac{1}{\varepsilon_{\boldsymbol{k}}}\right), \tag{6b}$$

where we have employed the renormalization relation for the s-wave coupling constant,

$$\frac{1}{g_{12}} = \frac{m}{4\pi\hbar^2 a_{12}} - \frac{1}{2V}\sum_{\boldsymbol{k}}\frac{1}{\varepsilon_{\boldsymbol{k}}}. \tag{7}$$

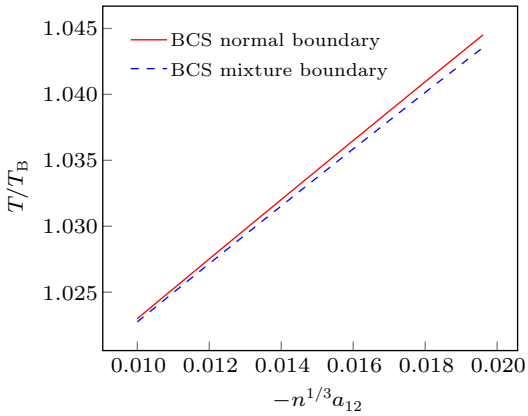


Fig. 1. Phase diagram of a binary Bose gas with intra-species gas parameter $n^{1/3}a_{11} = 0.02$, where the horizontal axis is the absolute value of the inter-species gas parameter $n^{1/3}|a_{12}|$. Here, n is the density of one species, a_{12} is the inter-species scattering length, and $T_{\rm B} = 2\pi\hbar^2 n^{2/3}/(mk_{\rm B}\zeta^{2/3}(3/2))$ is the ideal BEC temperature. Starting from the normal state, the system first transitions into the BCS state and then quickly evolves into a BEC–BCS mixture state. The normal–BCS and BCS–mixture transition temperatures are indicated by the red solid and blue dashed lines, respectively.

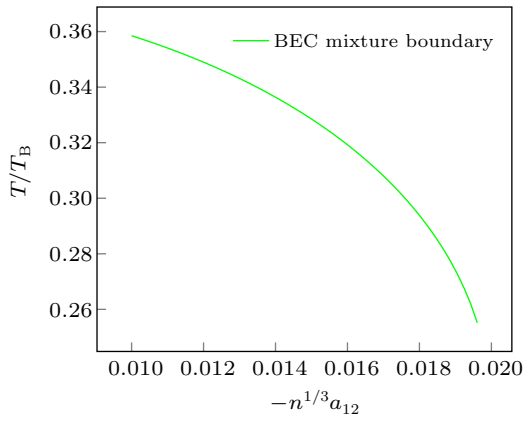


Fig. 2. Transition between the BEC–BCS mixture and BEC states for $n^{1/3}a_{11} = 0.02$. The system remains in the BEC–BCS mixture state over a wide temperature range. As the temperature decreases, the mixture state eventually transitions into the BEC state. The mixture–BEC transition temperature is indicated by the green solid line.

The BCS state exists between two critical temperatures, $T_{\rm C2} \le T \le T_{\rm C1}$, as shown by the numerical results in Fig. 1. At the first critical temperature $T_{\rm C1}$, the pairing order parameter Δ vanishes, marking a phase transition from the normal state to the BCS state. The critical temperature $T_{\rm C1}$ is determined by the following equation:

$$-\frac{m}{4\pi\hbar^2 a_{12}} = \int \frac{{\rm d}^3\boldsymbol{k}}{2(2\pi)^3}\left(\frac{1}{\varepsilon_{\boldsymbol{k}} - \mu'}\coth\frac{\varepsilon_{\boldsymbol{k}} - \mu'}{2k_{\rm B}T_{\rm C1}} - \frac{1}{\varepsilon_{\boldsymbol{k}}}\right). \tag{8}$$

The right-hand side of Eq. (8) exhibits an infrared divergence at $\mu' = 0$, which occurs when the temperature reaches

the ideal BEC temperature

$$T_{\mathrm{B}} = \frac{2\pi\hbar^2 n^{2/3}}{m k_{\mathrm{B}} \zeta^{2/3}\left(\frac{3}{2}\right)}.$$

This indicates that Eq. (8) always admits a solution with $T_{\mathrm{C1}} > T_{\mathrm{B}}$, regardless of how weak the inter-species interaction is. Therefore, upon cooling from the normal state, the system always first enters the BCS pairing phase before reaching the BEC state. For the parameters used in Fig. 3, the critical temperature T_{C1} is approximately $1.0414\,T_{\mathrm{B}}$.

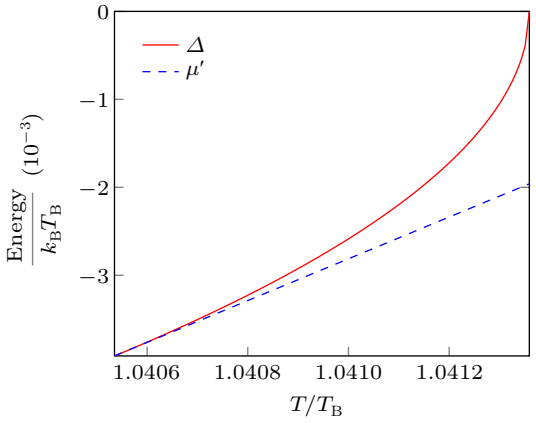


Fig. 3. Pairing order parameter Δ and shifted chemical potential μ' as functions of temperature for $n^{1/3}a_{11} = 0.02$ and $n^{1/3}a_{12} = -0.018$. $\Delta/k_{\mathrm{B}}T_{\mathrm{B}}$ and $\mu'/k_{\mathrm{B}}T_{\mathrm{B}}$ are indicated by red solid and blue dashed lines, respectively. As the temperature decreases, both Δ and $|\mu'|$ increase, while the energy gap E_0 decreases. The transition from the normal state to the BCS state occurs at $T_{\mathrm{C1}} \approx 1.0414T_{\mathrm{B}}$, and the transition from the BCS state to the BEC–BCS mixture state occurs at $T_{\mathrm{C2}} \approx 1.0405T_{\mathrm{B}}$.

In this BCS pairing state, as the temperature further decreases, both $|\mu'|$ and $|\Delta|$ increase, while the energy gap E_0 decreases, as shown in Fig. 3. At the second critical temperature T_{C2}, where $\mu' = \Delta$, the excitation gap vanishes ($E_0 = 0$). At this point, there is no energy cost for atoms to enter the condensate, and the system evolves into a mixed state consisting of BCS pairs and BEC atoms, which will be analyzed in the latter part of this work. It can be shown from Eqs. (6a) and (6b) that the critical temperature T_{C2} is also always higher than T_{B}. In Fig. 3, T_{C2} is approximately $1.0405T_{\mathrm{B}}$.

As shown in Fig. 1, in the dilute regime, both critical temperatures T_{C1} and T_{C2} are close to T_{B}. An interesting question is whether the critical fluctuations associated with condensation near T_{B} can substantially modify this phase diagram. The size of the critical region can be estimated using the Ginzburg criterion, defined as the deviation of the actual critical temperature from its mean-field value, ΔT_{B}. In Refs. [39,40], this deviation was calculated for a single-species Bose gas and attributed to two-loop self-energy diagrams. For a binary Bose gas, the same mechanism applies, and ΔT_{B} can be obtained by adopting the result from Ref. [40] with the replacement of the scattering length by $a = \sqrt{a_{11}^2 + a_{12}^2/2}$. As shown in Fig. 4, which compares the critical temperature deviations $\Delta T_{\mathrm{C1}} = T_{\mathrm{C1}} - T_{\mathrm{B}}$, $\Delta T_{\mathrm{C2}} = T_{\mathrm{C2}} - T_{\mathrm{B}}$, and ΔT_{B}, the BCS phase lies well outside the critical region near T_{B}, indicating that the mean-field approximation remains valid.

2.3. Pairing stability

To analyze the stability of the BCS pairing state, we apply Landau's theory of phase transitions.[17] The mean-field Helmholtz free energy is given by

$$\begin{aligned} F =\ & 2\sum_{\boldsymbol{k}}\left[E_{\boldsymbol{k}}\left(f_{\boldsymbol{k}}+\frac{1}{2}\right)-\frac{1}{2}\eta_{\boldsymbol{k}}\right] \\ & -2k_{\mathrm{B}}T\sum_{\boldsymbol{k}}\left[(f_{\boldsymbol{k}}+1)\ln(f_{\boldsymbol{k}}+1)-f_{\boldsymbol{k}}\ln f_{\boldsymbol{k}}\right] \\ & -\frac{\Delta^2 V}{g_{12}}-(2g_{11}+g_{12})n^2V+2\mu n, \end{aligned} \tag{9}$$

where $\eta_{\boldsymbol{k}} = \varepsilon_{\boldsymbol{k}} - \mu + (2g_{11}+g_{12})n$, $E_{\boldsymbol{k}} = \sqrt{\eta_{\boldsymbol{k}}^2 - \Delta^2}$ is the quasi-particle energy from Eq. (5), and $f_{\boldsymbol{k}}$ is the Bose distribution function of quasi-particles, $f_{\boldsymbol{k}} = \frac{1}{\mathrm{e}^{\beta E_{\boldsymbol{k}}}-1}$.

To examine the stability of the BCS state, we expand the free energy near the normal-state solution, $\mu = \mu_0$ and $\Delta = 0$, keeping the density n constant, where μ_0 is the chemical potential of the normal state. In terms of $\delta\mu = \mu - \mu_0$ and Δ, the free-energy difference between the BCS and normal states up to the quartic order in Δ is given by

$$\begin{aligned} & \delta F \\ =\ & \Delta^2\left[\frac{-V}{g_{12}}-\sum_{\boldsymbol{k}}\left(\frac{1}{2\eta_{\boldsymbol{k}0}}+\frac{\delta\mu}{2\eta_{\boldsymbol{k}0}^2}+\frac{\Delta^2}{8\eta_{\boldsymbol{k}0}^3}\right)\coth\left(\frac{\beta\eta_{\boldsymbol{k}0}}{2}\right)\right], \end{aligned} \tag{10}$$

where $\eta_{\boldsymbol{k}0} = \eta_{\boldsymbol{k}}|_{\mu=\mu_0}$.

The relationship between $\delta\mu$ and Δ can be obtained by taking the difference between both sides of Eq. (6a)

$$\delta\mu = \frac{\Delta^2\sum_{\boldsymbol{k}}\left(\frac{1}{2\eta_{\boldsymbol{k}0}^2}\left(f_{\boldsymbol{k}0}+\frac{1}{2}\right)-\frac{f'_{\boldsymbol{k}0}}{2\eta_{\boldsymbol{k}0}}\right)}{\sum_{\boldsymbol{k}} f'_{\boldsymbol{k}0}}, \tag{11}$$

where $f'_{\boldsymbol{k}0} = -\beta f_{\boldsymbol{k}0}^2\,\mathrm{e}^{\beta\eta_{\boldsymbol{k}0}}$. Therefore, the free-energy difference up to the quartic order in Δ between the BCS and normal states is given by

$$\delta F = \alpha'\Delta^2 + \beta'\Delta^4, \tag{12}$$

where

$$\begin{aligned} \alpha' &= -\frac{V}{g_{12}} - \sum_{\boldsymbol{k}}\frac{\coth\left(\frac{\beta\eta_{\boldsymbol{k}0}}{2}\right)}{2\eta_{\boldsymbol{k}0}}, \\ \beta' &= -2\sum_{\boldsymbol{k}}\left[\frac{\sum_{\boldsymbol{k}_1}\left(\frac{f_{\boldsymbol{k}_1 0}+\frac{1}{2}}{2\eta_{\boldsymbol{k}_1 0}^2}-\frac{f'_{\boldsymbol{k}_1 0}}{2\eta_{\boldsymbol{k}_1 0}}\right)}{2\eta_{\boldsymbol{k}0}^2\sum_{\boldsymbol{k}_2} f'_{\boldsymbol{k}_2 0}}+\frac{1}{8\eta_{\boldsymbol{k}0}^3}\right]\left(f_{\boldsymbol{k}0}+\frac{1}{2}\right). \end{aligned} \tag{13}$$

A stable BCS state requires the free energy to have a local minimum rather than a saddle point. It is clear from Eq. (6b)

that $\alpha' = 0$ at the BCS–normal transition point. Below the transition temperature T_{C1}, $\alpha' < 0$, and the stability condition requires $\beta' > 0$. In the dilute regime, $n|a_{ij}|^3 \ll 1$ and $\beta\eta_{00} \ll 1$, the coefficient β' is approximately given by

$$\beta' \approx \frac{V}{256\pi\eta_{00}^{\frac{5}{2}}\beta}\left(\frac{2m}{\hbar^2}\right)^{\frac{3}{2}} > 0, \tag{14}$$

and the stability condition is thus satisfied. As in the Ginzburg–Landau theory of superconductivity, the specific heat, obtained from the second derivative of δF with respect to temperature, exhibits a discontinuity at T_{C1}.

2.4. Pairing size

In the dilute region, both energies $|\mu'|$ and $|\Delta|$ are much smaller than $k_B T_B$, as shown in Fig. 3. The pair function is defined as

$$\chi(\boldsymbol{r}) = \frac{1}{V}\sum_{\boldsymbol{k}}\langle c_{1\boldsymbol{k}}c_{2-\boldsymbol{k}}\rangle e^{i\boldsymbol{k}\cdot\boldsymbol{r}}, \tag{15}$$

which can be obtained analytically in the large-distance limit, $r \gg n^{-1/3}$, as

$$\chi(\boldsymbol{r}) \approx \frac{mk_B T}{4\pi\hbar^2 r}\left(e^{-r/\xi} - e^{-r/\xi'}\right), \tag{16}$$

where the two characteristic lengths are given by $\xi = \left(2m|\mu' - \Delta|/\hbar^2\right)^{-1/2}$ and $\xi' = \left(2m|\mu' + \Delta|/\hbar^2\right)^{-1/2}$. In the dilute region, the pair size ξ is much larger than the interparticle distance, $\xi \gg n^{-1/3}$, indicating significant spatial overlap between pairs. Thus, the pairing state clearly lies in the BCS limit, opposite to the molecular BEC limit.

3. Mixture state

At the lower critical temperature T_{C2}, the energy gap preventing the BEC formation vanishes, i.e., $E_0 = 0$. Here we explore the possibility of a mixture state consisting of atomic BEC and phase-coherent inter-species pairs below T_{C2}. In this mixture state, two order parameters coexist: the BEC wavefunction $\psi_0 = \langle c_{i0}\rangle/\sqrt{V}$ and the pairing order parameter $\Delta = g_{12}\sum_{\boldsymbol{k}\neq 0}\langle c_{1\boldsymbol{k}}c_{2-\boldsymbol{k}}\rangle/V$. We consider the case where the BEC and the pairs are phase coherent, and assume $\psi_0 > 0$ without loss of generality. The mean-field thermodynamic potential is given by

$$\begin{aligned}\Omega_0 &= \langle H_I - \mu N\rangle \\ &= V\Big\{g_{11}\left[n_0^2 + \tilde{n}(4n_0 + 2\tilde{n})\right] + g_{12}\Big[\tilde{n}(2n_0 + \tilde{n}) \\ &\quad + \Big|n_0 + \frac{\Delta}{g_{12}}\Big|^2\Big] - 2\mu(n_0 + \tilde{n})\Big\},\end{aligned} \tag{17}$$

where $n_0 = \psi_0^2$ is the condensate density of one component, and $\tilde{n} = n - n_0$ is the non-condensed atom density of the same component. For attractive inter-species interaction $g_{12} < 0$, Ω_0 reaches its minimum when Δ and $g_{12}n_0$ have the same sign. Thus, the condensate and the pairs are phase coherent, and in the following we take Δ as a negative parameter. The chemical potential μ is determined from the stationary condition $\frac{\partial\Omega_0}{\partial n_0}|_{\tilde{n},\Delta} = 0$, yielding

$$\mu = (g_{11} + g_{22})n_0 + (2g_{11} + g_{12})\tilde{n} + \Delta. \tag{18}$$

Including the Hartree–Fock and pairing energies, the mean-field Hamiltonian in the grand-canonical ensemble is

$$\begin{aligned}H_M - \mu N = E_M + \sum_{\boldsymbol{k}\neq 0}\Big[&\left(\varepsilon_{\boldsymbol{k}} - \mu'\right)\left(c_{1\boldsymbol{k}}^\dagger c_{1\boldsymbol{k}} + c_{2\boldsymbol{k}}^\dagger c_{2\boldsymbol{k}}\right) \\ &+ \frac{g_{11}n_0}{2}\left(c_{1\boldsymbol{k}}^\dagger c_{1-\boldsymbol{k}}^\dagger + c_{2\boldsymbol{k}}^\dagger c_{2-\boldsymbol{k}}^\dagger + \text{h.c.}\right) \\ &+ g_{12}n_0\left(c_{1\boldsymbol{k}}^\dagger c_{2\boldsymbol{k}} + \text{h.c.}\right) \\ &+ (\Delta + g_{12}n_0)\left(c_{1\boldsymbol{k}}c_{2-\boldsymbol{k}} + \text{h.c.}\right)\Big],\end{aligned} \tag{19}$$

where

$$\frac{E_M}{V} = g_{11}\left(n_0^2 - 2\tilde{n}^2\right) + g_{12}\left[n_0^2 - \tilde{n}^2 - \left(\frac{\Delta}{g_{12}}\right)^2\right] - 2\mu n_0,$$

and $\mu' = \mu - (2g_{11} + g_{12})n$ as defined previously. There are important differences between Eq. (19) and the Hamiltonian proposed for the pairing state in quantum droplets.[37,38] In Eq. (19), the Hartree–Fock contribution from the inter-species interaction is included, and the mean-field term from the non-condensed atoms is taken into account as in Popov's approximation.[41] Therefore, Eq. (19) is capable of describing all three broken-symmetry states: BEC, BCS, and mixture states. When $\Delta = 0$, Eq. (19) reduces to the Bogoliubov Hamiltonian for the BEC state; when $n_0 = 0$, it reproduces the BCS-state Hamiltonian, Eq. (4).

After the canonical transformation $\alpha_{\boldsymbol{k}}^\dagger = \frac{1}{\sqrt{2}}\left(c_{1\boldsymbol{k}}^\dagger + c_{2\boldsymbol{k}}^\dagger\right)$ and $\beta_{\boldsymbol{k}}^\dagger = \frac{1}{\sqrt{2}}\left(c_{1\boldsymbol{k}}^\dagger - c_{2\boldsymbol{k}}^\dagger\right)$, Eq. (19) becomes

$$\begin{aligned}&H_M - \mu N \\ &= \frac{1}{2}\sum_{\boldsymbol{k}\neq 0}\Big[\left(\varepsilon_{\boldsymbol{k}} - \mu' + g_{12}n_0\right)\left(\alpha_{\boldsymbol{k}}^\dagger\alpha_{\boldsymbol{k}} + \alpha_{-\boldsymbol{k}}^\dagger\alpha_{-\boldsymbol{k}}\right) \\ &\quad + \left((g_{11} + g_{12})n_0 + \Delta\right)\left(\alpha_{\boldsymbol{k}}^\dagger\alpha_{-\boldsymbol{k}}^\dagger + \text{h.c.}\right)\Big] \\ &\quad + \frac{1}{2}\sum_{\boldsymbol{k}\neq 0}\Big[\left(\varepsilon_{\boldsymbol{k}} - \mu' - g_{12}n_0\right)\left(\beta_{\boldsymbol{k}}^\dagger\beta_{\boldsymbol{k}} + \beta_{-\boldsymbol{k}}^\dagger\beta_{-\boldsymbol{k}}\right) \\ &\quad + \left((g_{11} - g_{12})n_0 - \Delta\right)\left(\beta_{\boldsymbol{k}}^\dagger\beta_{-\boldsymbol{k}}^\dagger + \text{h.c.}\right)\Big] + E_M.\end{aligned} \tag{20}$$

The mean-field Hamiltonian in Eq. (20) can be diagonalized by a Bogoliubov transformation, yielding two excitation branches. The density excitation energy is

$$E_{\boldsymbol{k}+} = \sqrt{\left(\varepsilon_{\boldsymbol{k}} - \mu' + g_{12}n_0\right)^2 - \left[(g_{11} + g_{12})n_0 + \Delta\right]^2}, \tag{21}$$

and the spin excitation energy is

$$E_{\boldsymbol{k}-} = \sqrt{\left(\varepsilon_{\boldsymbol{k}} - \mu' - g_{12}n_0\right)^2 - \left[(g_{11} - g_{12})n_0 - \Delta\right]^2}. \tag{22}$$

Substituting the chemical potential from Eq. (18), we obtain

the final expressions for the excitation energies

$$E_{\boldsymbol{k}+} = \sqrt{(\varepsilon_{\boldsymbol{k}} - 2\Delta)\left[\varepsilon_{\boldsymbol{k}} + 2(g_{11}+g_{12})n_0\right]}, \tag{23}$$

$$E_{\boldsymbol{k}-} = \sqrt{\varepsilon_{\boldsymbol{k}}\left[\varepsilon_{\boldsymbol{k}} + 2(g_{11}-g_{12})n_0 - 2\Delta\right]}. \tag{24}$$

The density excitation is gapped, as in the BCS state, while the spin excitation is gapless, consistent with Refs. [37,38], though the detailed spectrum differs. In particular, the density-excitation energy $E_{\boldsymbol{k}+}$ becomes unstable at the mean-field instability point $g_{11}+g_{12}=0$. This difference arises from the inclusion of the Hartree–Fock term for the inter-species interaction in our treatment.

The condensate density n_0 and the pairing order parameter Δ are determined self-consistently from

$$\frac{\Delta}{4\pi\hbar^2 a_{12}/m} = \int \frac{\mathrm{d}^3\boldsymbol{k}}{2(2\pi)^3}\left\{\left[\sum_{\pm} \pm \frac{g_{11}n_0 \pm (\Delta + g_{12}n_0)}{2E_{\boldsymbol{k}\pm}}\left(2f_{\boldsymbol{k}\pm}+1\right)\right] + \frac{\Delta + g_{12}n_0}{\varepsilon_{\boldsymbol{k}}}\right\}, \tag{25a}$$

$$n_0 = n - \int \frac{\mathrm{d}^3\boldsymbol{k}}{2(2\pi)^3}\sum_{\pm}\left[\frac{\varepsilon_{\boldsymbol{k}} + (g_{11} \pm g_{12})n_0 - \Delta}{2E_{\boldsymbol{k}\pm}}\left(f_{\boldsymbol{k}\pm}+\frac{1}{2}\right) - \frac{1}{2}\right], \tag{25b}$$

where $\sum_{\pm}$ denotes the summation over the two branches, and $f_{\boldsymbol{k}\pm} = (\mathrm{e}^{\beta E_{\boldsymbol{k}\pm}} - 1)^{-1}$ are the Bose distribution functions of the quasiparticles.

The numerical solutions of these two equations are shown in Fig. 4. As the temperature decreases below the critical temperature T_{C2}, the condensation fraction n_0/n increases, and the pairing amplitude $|\Delta|$ decreases after a brief increase, showing that the mixture state evolves towards the BEC state. At low temperatures, the pairing order parameter is almost negligible and a transition into the BEC state is likely to occur. In Fig. 5, this transition temperature is approximately given by $T_{\mathrm{C3}} \approx 0.2908 T_{\mathrm{B}}$ with the specific parameters. When $\Delta = 0$, Eq. (25b) recovers the number equation of the BEC state.[41]

In the region below the ideal BEC temperature T_{B}, the mixture state competes with the BEC state. We numerically compare the chemical potential of the BEC state with that of the mixture state from Eq. (18) in Fig. 6. As shown in Fig. 6, above the transition temperature $T_{\mathrm{C3}} \approx 0.29079 T_{\mathrm{B}}$, the chemical potential of the mixture state is lower than that of the BEC state, and is thus more favored and stable. As the temperature continues to decrease below T_{C3}, there are no numerical solutions for Eqs. (25a) and (25b), indicating the

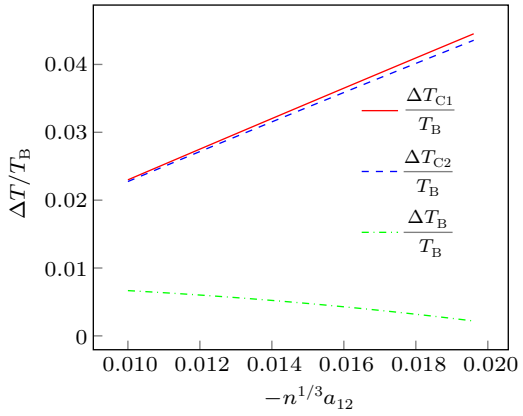


Fig. 4. BCS–normal transition temperature T_{C1}, normal–mixture transition temperature T_{C2}, and the correction to the BEC transition temperature ΔT_{B} as functions of the inter-species gas parameter, calculated at fixed intra-species gas parameter $n^{1/3}a_{11} = 0.02$. Here, $\Delta T_{\mathrm{C1}} = T_{\mathrm{C1}} - T_{\mathrm{B}}$ and $\Delta T_{\mathrm{C2}} = T_{\mathrm{C2}} - T_{\mathrm{B}}$ denote the upper and lower boundaries of the BCS phase, respectively. ΔT_{B} represents the shift of the condensation temperature due to critical fluctuations. It is evident that the BCS phase lies well outside the critical region of condensation.

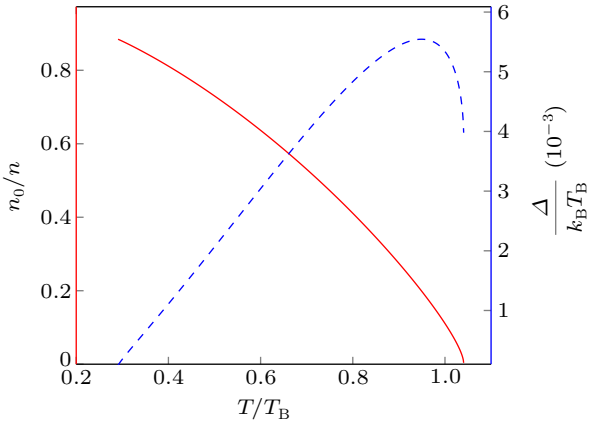


Fig. 5. BEC fraction n_0/n and pairing amplitude $|\Delta|/(k_{\mathrm{B}}T_{\mathrm{B}})$ versus temperature in the mixture state, numerically calculated for $n^{1/3}a_{11} = 0.02$ and $n^{1/3}a_{12} = -0.018$. The BEC fraction n_0/n and pairing amplitude $|\Delta|/(k_{\mathrm{B}}T_{\mathrm{B}})$ are shown by the red-solid and blue-dashed lines, respectively. As the temperature approaches the transition temperature $T_{\mathrm{C3}} \approx 0.2908\,T_{\mathrm{B}}$, the BEC fraction increases while the pairing amplitude decreases, indicating a crossover of the system into the BEC state.

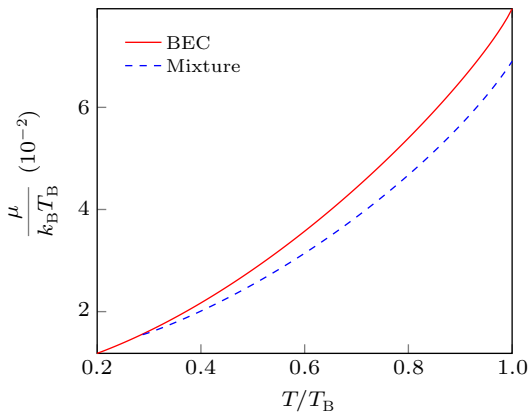


Fig. 6. Chemical potential μ in the mixture and BEC states versus temperature for $n^{1/3}a_{11} = 0.02$ and $n^{1/3}a_{12} = -0.018$. The chemical potentials $\mu_{\mathrm{BEC}}/(k_{\mathrm{B}}T_{\mathrm{B}})$ and $\mu_{\mathrm{mixture}}/(k_{\mathrm{B}}T_{\mathrm{B}})$ are shown by the red-solid and blue-dashed lines, respectively. The phase transition from the mixture state to the BEC state occurs at approximately $T_{\mathrm{C3}} \approx 0.2908\,T_{\mathrm{B}}$.

disappearance of the mixture state and the emergence of the BEC state.

4. Discussion and conclusion

Quantum droplets have been experimentally realized in homonuclear ^{39}K binary gases[29,42,43] in the mean-field-unstable region with $-a_{12} > \sqrt{a_{11}a_{22}}$, where the LHY energy is of the same order as the mean-field energy. Although the ^{39}K system generally has asymmetric intra-species interactions, our results about the BCS state can still be tested by tuning the detuning energy $\delta = 2(g_{11} - g_{22})n$ in the second component, so that both components are equally populated, equivalent to the symmetric case, while the mixture state is more complicated. As shown in Fig. 1, in the dilute region, the BCS state occupies a narrow region, which may be difficult to observe. In contrast, the mixture state exists in a much wider region, making it more suitable for experimental observation.

Currently, spectroscopic methods, originally developed in solid-state systems such as angle-resolved photoemission spectroscopy (ARPES) and neutron scattering, have been successfully applied to ultracold atoms. Radio-frequency (RF) spectroscopy[44–46] and Bragg spectroscopy[47] can already provide energy-resolved insights into our binary bosonic system. The BEC, BCS, and mixture states can be distinguished via their excitation spectra. In the BEC state, both spin and density excitations are degenerate and gapless; in the BCS state, both excitations are degenerate with the energy gap $E_0 = \sqrt{\mu'^2 - \Delta^2}$; in the mixture state, the spin excitation is gapless, while the density excitation is gapped by $E_{0+} = \sqrt{4|\Delta|(g_{11}+g_{12})n_0}$. For the parameters used in Fig. 3 and Fig. 5, the maximum E_0 is of the order of $10^{-3}k_{\mathrm{B}}T_{\mathrm{B}}$, and the maximum E_{0+} is of the order of $10^{-2}k_{\mathrm{B}}T_{\mathrm{B}}$. These three states also exhibit differences in their topological excitations. In a vortex of the BEC state, the angular momentum per atom in the condensate is $\hbar$; in a vortex of the BCS state, the angular momentum per paired atom is reduced to half.

The mixture state in the mean-field stable region is qualitatively similar to the pairing state in the mean-field unstable region proposed for quantum droplets[37]. Both states contain atomic condensation and inter-species pairs but are subject to slightly different treatments. Here, we have included all Hartree–Fock energies, especially the inter-species Hartree–Fock term, which was omitted in Refs. [37,38]. The mixture state exists only at finite temperatures and is eventually taken over by the BEC state at low temperatures. In contrast, the pairing state of the quantum droplet exists at zero temperature and is destabilized at a finite temperature[48]. Our result on pairing bosons could be related to fermionic quartets[49].

In conclusion, we have obtained the phase diagram of a symmetric Bose gas with attractive inter-species interactions in the mean-field stable region, identifying three pairing-related phase transitions. As the temperature decreases, the system first transitions from the normal state to the BCS pairing state. With further cooling, a phase transition from the BCS state to a mixture of BEC and pairs occurs. At an even lower temperature, the mixture state is replaced by the BEC state. Our results may be tested in current experimental setups.

Acknowledgment

We would like to thank T.-L. Ho, Z.-Q. Yu, and Q. Gu for helpful discussions.

References

[1] Anderson M H, Ensher J R, Matthews M R, Wieman C E and Cornell E A 1995 *Science* **269** 198
[2] Davis K B, Mewes M O, Andrews M R, van Druten N J, Durfee D S, Kurn D M and Ketterle W 1995 *Phys. Rev. Lett.* **75** 3969
[3] Eagles D M 1969 *Phys. Rev.* **186** 456
[4] Giorgini S, Pitaevskii L P and Stringari S 2008 *Rev. Mod. Phys.* **80** 1215
[5] Greiner M, Regal C A and Jin D S 2003 *Nature* **426** 537
[6] Zwierlein M W, Stan C A, Schunck C H, Raupach S M F, Gupta S, Hadzibabic Z and Ketterle W 2003 *Phys. Rev. Lett.* **91** 250401
[7] Jochim S, Bartenstein M, Altmeyer A, Hendl G, Riedl S, Chin C, Denschlag J H and Grimm R 2003 *Science* **302** 2101
[8] Regal C A, Greiner M and Jin D S 2004 *Phys. Rev. Lett.* **92** 040403
[9] Chin C, Bartenstein M, Altmeyer A, Riedl S, Jochim S, Denschlag J H and Grimm R 2004 *Science* **305** 1128
[10] Kinast J, Hemmer S L, Gehm M E, Turlapov A and Thomas J E 2004 *Phys. Rev. Lett.* **92** 150402
[11] Zwierlein M W, Stan C A, Schunck C H, Raupach S M F, Kerman A J and Ketterle W 2004 *Phys. Rev. Lett.* **92** 120403
[12] Bourdel T, Khaykovich L, Cubizolles J, Zhang J, Chevy F, Teichmann M, Tarruell L, Kokkelmans S J J M F and Salomon C 2004 *Phys. Rev. Lett.* **93** 050401
[13] Bartenstein M, Altmeyer A, Riedl S, Jochim S, Chin C, Denschlag J H and Grimm R 2004 *Phys. Rev. Lett.* **92** 120401
[14] Zwierlein M W, Abo-Shaeer J R, Schirotzek A, Schunck C H and Ketterle W 2005 *Nature* **435** 1047
[15] Bardeen J, Cooper L N and Schrieffer J R 1957 *Phys. Rev.* **106** 162
[16] Evans W A B and Rashid R I M A 1973 *J. Low Temp. Phys.* **11** 93
[17] Jeon G S, Yin L, Rhee S W and Thouless D J 2002 *Phys. Rev. A* **66** 011603
[18] Stoof H T C 1994 *Phys. Rev. A* **49** 3824
[19] Mueller E J and Baym G 2000 *Phys. Rev. A* **62** 053605
[20] Yu Z Q and Yin L 2010 *Phys. Rev. A* **81** 023613
[21] Radzihovsky L, Park J and Weichman P B 2004 *Phys. Rev. Lett.* **92** 160402
[22] Nozières, P and Saint James D 1982 *J. Phys. France* **43** 1133
[23] Stenger J, Inouye S, Andrews M R, Miesner H J, Stamper-Kurn D M and Ketterle W 1999 *Phys. Rev. Lett.* **82** 2422
[24] Bonnes L and Wessel S 2011 *Phys. Rev. Lett.* **106** 185302
[25] Chen Y C, Ng K K and Yang M F 2011 *Phys. Rev. B* **84** 092503
[26] Sowiński T, Chhajlany R W, Dutta O, Tagliacozzo L and Lewenstein M 2015 *Phys. Rev. A* **92** 043615
[27] Zhang Z, Chen L, Yao K X and Chin C 2021 *Nature* **592** 708
[28] Cabrera C R, Tanzi L, Sanz J, Naylor B, Thomas P, Cheiney P and Tarruell L 2018 *Science* **359** 301
[29] Cheiney P, Cabrera C R, Sanz J, Naylor B, Tanzi L and Tarruell L 2018 *Phys. Rev. Lett.* **120** 135301
[30] Semeghini G, Ferioli G, Masi L, Mazzinghi C, Wolswijk L, Minardi F, Modugno M, Modugno G, Inguscio M and Fattori M 2018 *Phys. Rev. Lett.* **120** 235301
[31] Petrov D S 2018 *Nat. Phys.* **14** 211
[32] Petrov D S 2015 *Phys. Rev. Lett.* **115** 155302
[33] Gu Q and Yin L 2020 *Phys. Rev. B* **102** 220503
[34] Xiong Y and Yin L 2022 *Phys. Rev. A* **105** 053305
[35] Zhang F and Yin L 2022 *Chin. Phys. Lett.* **39** 060301
[36] Zhang F and Yin L 2025 *Chin. Phys. Lett.* **42** 010302

[37] Hu H and Liu X J 2020 *Phys. Rev. Lett.* **125** 195302
[38] Hu H, Wang J and Liu X J 2020 *Phys. Rev. A* **102** 043301
[39] Baym G, Blaizot J P, Holzmann M, Laloë F and Vautherin D 1999 *Phys. Rev. Lett.* **83** 1703
[40] Holzmann M, Baym G, Blaizot J P and Laloë F 2001 *Phys. Rev. Lett.* **87** 120403
[41] Ota M and Giorgini S 2020 *Phys. Rev. A* **102** 063303
[42] Cabrera C R, Tanzi L, Sanz J, Naylor B, Thomas P, Cheiney P and Tarruell L 2018 *Science* **359** 301
[43] Semeghini G, Ferioli G, Masi L, Mazzinghi C, Wolswijk L, Minardi F, Modugno M, Modugno G, Inguscio M and Fattori M 2018 *Phys. Rev. Lett.* **120** 235301
[44] Stewart J T, Gaebler J P and Jin D S 2008 *Nature* **454** 744
[45] Wild R J, Makotyn P, Pino J M, Cornell E A and Jin D S 2012 *Phys. Rev. Lett.* **108** 145305
[46] Shashi A, Grusdt F, Abanin D A and Demler E 2014 *Phys. Rev. A* **89** 053617
[47] Papp S B, Pino J M, Wild R J, Ronen S, Wieman C E, Jin D S and Cornell E A 2008 *Phys. Rev. Lett.* **101** 135301
[48] Wang J, Hu H and Liu X J 2020 *New J. Phys.* **22** 103044
[49] Volovik G E 2024 *JETP Lett.* **119** 330